Brain IRS2 Signaling Coordinates Life Span and Nutrient Homeostasis

Akiko Taguchi *et al.*

Science **317**, 369 (2007);
DOI: 10.1126/science.1142179

could, in a multicellular organism, be controlled at the level of gene coexpression and protein colocalization, our results indicate that the intrinsic selectivity of PDZ domains is tuned across the mouse proteome to minimize cross-reactivity.

Finally, we observed only a weak correlation (correlation coefficient $r = 0.23$) between the pairwise sequence divergence of PDZ domains and their distances in selectivity space (Fig. 3H). Similarity at the overall sequence level is thus a poor predictor of PDZ domain function. This low correlation suggests that most of the sequence variation among PDZ domains is neutral with respect to peptide-binding selectivity and that only a subset of residues—presumably in the binding pocket of the PDZ domain—is responsible for the distribution of PDZ domains in selectivity space.

References and Notes

1. T. Pawson, *Nature* **373**, 573 (1995).
2. T. Pawson, P. Nash, *Science* **300**, 445 (2003).
3. E. Kim, M. Niethammer, A. Rothschild, Y. N. Jan, M. Sheng, *Nature* **378**, 85 (1995).
4. H. C. Kornau, L. T. Schenker, M. B. Kennedy, P. H. Seeburg, *Science* **269**, 1737 (1995).
5. C. Nourry, S. G. N. Grant, J.-P. Borg, *Sci. STKE* **2003**, re7 (2003).
6. B. Z. Harris, F. W. Lau, N. Fujii, R. K. Guy, W. A. Lim, *Biochemistry* **42**, 2797 (2003).
7. Z. Songyang *et al.*, *Science* **275**, 73 (1997).
8. I. Bezprozvanny, A. Maximov, *FEBS Lett.* **509**, 457 (2001).
9. E. Song *et al.*, *Mol. Cell. Proteomics* **5**, 1368 (2006).
10. I. Letunic *et al.*, *Nucleic Acids Res.* **34**, D257 (2006).
11. J. Schultz, F. Milpetz, P. Bork, C. P. Ponting, *Proc. Natl. Acad. Sci. U.S.A.* **95**, 5857 (1998).
12. The "genomic" mode of the Simple Modular Architecture Research Tool (SMART) database (*10*, *11*) currently lists 240 PDZ domains identified from the mouse genome sequence. We obtained sequence-verified clones for 203 of them. In addition, we cloned 18 PDZ domains that are listed only in the "normal" mode of the SMART database. Each domain was purified in a single step from a large-scale bacterial culture, its purity was assessed by SDS–polyacrylamide gel electrophoresis (fig. S1), and its aggregation state was assessed by analytical gel filtration (table S1). Soluble protein of the correct molecular weight was obtained for 157 PDZ domains. Of these, 151 were monomeric, 4 were dimeric, and 2 were a mixture of monomers and dimers (table S1).
13. G. Fuh *et al.*, *J. Biol. Chem.* **275**, 21486 (2000).
14. Y. Zhang *et al.*, *J. Biol. Chem.* **281**, 22299 (2006).
15. We derived 57 of the training-set peptides from proteins that had previously been shown to interact with PDZ domains. To allow for the possibility of discovering sequences that fall outside the established view of peptide-binding selectivity, we derived the other peptides from different members of 13 families of membrane proteins, regardless of whether their C termini feature canonical PDZ domain binding motifs (table S2).
16. R. B. Jones, A. Gordus, J. A. Krall, G. MacBeath, *Nature* **439**, 168 (2006).
17. M. A. Stiffler, V. P. Grantcharova, M. Sevecka, G. MacBeath, *J. Am. Chem. Soc.* **128**, 5913 (2006).
18. Data for each PDZ-peptide combination [FP, recorded as millipolarization (mP) units] were fit to an equation that describes saturation binding, as previously noted (*17*). Interactions were scored as "positive" if all three of the following criteria were met: (i) The data fit well to the equation ($r^2 > 0.95$); (ii) the difference between FP at 20 μM PDZ domain and FP at 0 μM PDZ domain was >15 mP units; and (iii) the K_d was <100 μM.
19. To estimate the false-negative rate of our microarray assay, we randomly selected 32 PDZ domains and 32 peptides. We then screened all 1024 possible interactions with the use of a single-point FP assay and determined the K_d for all positive interactions. A comparison of the resulting interaction matrix with the microarray data showed a false-negative rate of 6.6%.
20. J. C. Obenauer, L. C. Cantley, M. B. Yaffe, *Nucleic Acids Res.* **31**, 3635 (2003).
21. M. Sandberg, L. Eriksson, J. Jonsson, M. Sjostrom, S. Wold, *J. Med. Chem.* **41**, 2481 (1998).
22. Materials and methods are available as supporting material on *Science* Online.
23. S. van Dongen, thesis, University of Utrecht, Netherlands (2000).
24. Full-length sequences of 31,302 unique mouse proteins (including splicing variants) were downloaded with BioMart from data set NCBIM36 (*Mus musculus* genes) of Ensembl 44. The C-terminal sequence of each entry was extracted using a Python script.
25. Interactions in table S5 are model predictions with *m* set to 20. On the basis of the results of our model validation efforts, we estimate these predictions to have a true-positive rate of 35%, a false-positive rate of 7%, and a TP/FP ratio of 0.83.
26. This single-point assay measures the difference between FP at 20 nM peptide, 20 μM PDZ domain and FP at 20 nM peptide, 0 μM PDZ domain. An analysis of 1710 FP titration curves shows that applying a threshold of 40 mP units to this single-point assay correctly identifies 91% of the positives and 96% of the negatives (fig. S3). Thus, instead of performing an additional 1170 titration curves, we used this single-point assay with a threshold of 40 mP units to evaluate interactions between the 48 test peptides and the 74 PDZ domains in the MDSM.
27. R. Jansen *et al.*, *Science* **302**, 449 (2003).
28. A. Tropsha, *Annu. Rep. Comput. Chem.* **2**, 113 (2006).
29. G. Birrane, J. Chung, J. A. Ladias, *J. Biol. Chem.* **278**, 1399 (2003).
30. F. Jaulin-Bastard *et al.*, *J. Biol. Chem.* **277**, 2869 (2002).
31. F. Jaulin-Bastard *et al.*, *J. Biol. Chem.* **276**, 15256 (2001).
32. A. Zarrinpar, S. H. Park, W. A. Lim, *Nature* **426**, 676 (2003).

33. We thank A. Tropsha for valuable suggestions and the Faculty of Arts and Sciences Center for Systems Biology for support with instrumentation and automation. This work was supported by awards from the Smith Family Foundation, the Arnold and Mabel Beckman Foundation, and the W. M. Keck Foundation and by a grant from the NIH (1 RO1 GM072872-01). M.A.S. was supported in part by the NIH Molecular, Cellular, and Chemical Biology Training Grant (5 T32 GM07598-25), and J.R.C. was the recipient of a Corning CoStar fellowship.

Supporting Online Material

www.sciencemag.org/cgi/content/full/317/5836/364/DC1
Materials and Methods
Figs. S1 to S6
Tables S1 to S6
References

3 May 2007; accepted 19 June 2007
10.1126/science.1144592

Brain IRS2 Signaling Coordinates Life Span and Nutrient Homeostasis

Akiko Taguchi, Lynn M. Wartschow, Morris F. White*

Reduced insulin-like signaling extends the life span of *Caenorhabditis elegans* and *Drosophila*. Here, we show that, in mice, less insulin receptor substrate–2 (Irs2) signaling throughout the body or just in the brain extended life span up to 18%. At 22 months of age, brain-specific *Irs2* knockout mice were overweight, hyperinsulinemic, and glucose intolerant; however, compared with control mice, they were more active and displayed greater glucose oxidation, and during meals they displayed stable superoxide dismutase–2 concentrations in the hypothalamus. Thus, less Irs2 signaling in aging brains can promote healthy metabolism, attenuate meal-induced oxidative stress, and extend the life span of overweight and insulin-resistant mice.

Reaching old age in good health is not just good luck but the result of a favorable balance between hundreds of disease-causing and longevity-promoting genes; regardless, some common mechanisms that influence life span have emerged (*1*). First, calorie restriction reliably increases animal longevity, and second, reduced insulin-like signaling extends life span in *Caenorhabditis elegans* and *Drosophila melanogaster* (*2*, *3*). Calorie restriction and reduced insulin-like signaling might be linked because fasting reduces the intensity and duration of insulin secretion required for glucose homeostasis, and reduced insulin-like signaling promotes the expression of antioxidant enzymes that are associated with longevity (*3*–*5*). Adapting these principles to humans is challenging because calorie restriction is difficult and because reduced insulin-like signaling can be associated with small stature, metabolic disease, and diabetes.

Insulin and insulin-like growth factor-1 (IGF1) bind to receptors on the surface of all cells that phosphorylate tyrosyl residues on the insulin receptor substrates (IRSs)—chico in *Drosophila* and Irs1, -2, -3, and -4 in mammals. This signaling cascade activates the phosphoinositide-3-kinase (Pik3C) and the thymoma viral proto-oncogene Akt, which regulates many cellular processes, including the inactivation of forkhead box O1 (FoxO1) transcription factor (*6*). Reduced *chico* expression decreases brain and body growth while increasing life span up to 50%, which is related to the increased activity of dFOXO in *Drosophila* (*7*, *8*). In mice, the deletion of Irs1 reduces body growth and causes hyperinsulinemia, whereas the deletion of Irs2 ($Irs2^{-/-}$ mice) reduces brain growth and causes

Howard Hughes Medical Institute, Division of Endocrinology, Children's Hospital Boston, Harvard Medical School, Boston, MA 02115, USA.

*To whom correspondence should be addressed. E-mail: morris.white@childrens.harvard.edu

fatal diabetes by 3 months of age because of pancreatic β cell failure (*9*). By comparison, young (2-months-old) *Irs2*$^{+/-}$ mice display normal metabolic phenotypes (*10*). Old (22½-months-old) *Irs2*$^{+/-}$ mice were slightly heavier than wild-type (WT) mice, although young and old WT and *Irs2*$^{+/-}$ mice consumed the same amount of food each day (Fig. 1, A and B). In addition, old *Irs2*$^{+/-}$ mice were more insulin sensitive than old WT mice (Fig. 1C) because their fasting insulin and glucose concentrations were lower (fig. S1, A and B).

Because insulin sensitivity is associated with longevity (*3*), we compared the life spans of WT and *Irs2*$^{+/-}$ mice. Inspection of the results suggested that the date of birth (DOB), paternal (PID) and maternal (MID) identity, and sex influenced life span (table S1); therefore, we used semiparametric (Cox) and parametric regression to control the covariates and evaluate the effect of Irs2 (*11*). Cox regression revealed a 48-fold ($P < 10^{-9}$) reduced risk of death for *Irs2*$^{+/-}$ mice compared with WT controls (Fig. 1D and table S3). By using parametric analysis, we found that the median life span for *Irs2*$^{+/-}$ mice was 17% longer [for WT, median = 789 days and 95% confidence interval (CI) 755 to 769; for *Irs2*$^{+/-}$, median = 925 days and 95% CI 887 to 940; $P = 0.01$] (table S4). The maximum life span, estimated at the 90th percentile, increased similarly (for WT, 837 days and 95% CI 801 to 845; for *Irs2*$^{+/-}$, 982 days and 95% CI 935 to 998) (Fig. 1D and table S4).

Irs2 is expressed throughout the body (Fig. 2A) and many regions of the brain, including the cerebrum, the cerebellum, and the arcuate and paraventricular nuclei of the hypothalamus (fig. S2) (*12*, *13*). Reduced insulin-like signaling in neurons increases the life span of *C. elegans* and *Drosophila*, so it is possible that reduced neuronal Irs2 could extend mouse life span (*3*, *14*, *15*). To test this hypothesis, we deleted one (*bIrs2*$^{+/-}$) or both (*bIrs2*$^{-/-}$) loxP-flanked *Irs2* alleles (*fIrs2*-alleles) in the brain by intercrossing *fIrs2* mice with nestin-cre transgenic mice (*13*). Polymerase chain reaction (PCR) analysis confirmed that *Irs2* RNA was retained in all tested tissues of the *bIrs2*$^{-/-}$ mice except for the brain (Fig. 2A). Quantitative reverse transcription PCR (RT-PCR) confirmed that *Irs2* RNA was reduced about 50% in *bIrs2*$^{+/-}$ brains and more than 90% in *bIrs2*$^{-/-}$ brains compared with that of control *fIrs2* mice (Fig. 2A). By contrast, *Irs2* RNA increased in the pancreas of *bIrs2*$^{+/-}$ and *bIrs2*$^{-/-}$ mice, confirming that nestin-cre expression did not take place in pancreatic β cells (Fig. 2A).

Crosses between *bIrs2*$^{+/-}$ mice produced offspring at a normal frequency, whereas crosses between *bIrs2*$^{+/-}$ and *bIrs2*$^{-/-}$ mice produced fewer offspring; offspring were never produced by crossing *bIrs2*$^{-/-}$ mice (fig. S3A). Old male and female *bIrs2*$^{-/-}$ mice consumed the most food each day by comparison to the other mice (Fig. 2B). However, by 22 months the *bIrs2*$^{+/-}$ and *bIrs2*$^{-/-}$ mice were about 10 g heavier than controls, owing in part to increased adiposity (fig. S3, B and C). The *bIrs2*$^{-/-}$ mice were 10% longer, and their brains were 30% smaller than those of *fIrs2* or *bIrs2*$^{+/-}$ mice (fig. S3, D and E). These results support previous conclusions that brain Irs2 signaling promotes embryonic brain growth, central nutrient homeostasis, melanocortin 4 receptor signaling (body length), and fertility (*13*, *16*–*18*).

Control *fIrs2* mice developed insulin resistance between 2 and 22 months of age (Fig. 2C). Unlike old *Irs2*$^{+/-}$ mice (Fig. 1), old *bIrs2*$^{+/-}$ mice and young and old *bIrs2*$^{-/-}$ mice were insulin resistant (Fig. 2C). All the insulin-resistant mice displayed mild glucose intolerance (Fig. 2D). However, diabetes did not develop in these mice because insulin concentrations increased to compensate for peripheral resistance, reaching the highest amount in old male *bIrs2*$^{+/-}$ and *bIrs2*$^{-/-}$ mice (Fig. 2E). Consistent with the observed hyperinsulinemia, pancreatic islets were larger in old male *bIrs2*$^{+/-}$ and *bIrs2*$^{-/-}$ mice than in old controls (Fig. 2F).

Next, we compared the life spans of *fIrs2*, *bIrs2*$^{+/-}$, and *bIrs2*$^{-/-}$ mice by using semiparametric (Cox) and parametric regression to control for the covariates (table S2). Although *bIrs2*$^{+/-}$ and *bIrs2*$^{-/-}$ mice displayed metabolic changes usually associated with a shorter life span, their risk of death determined by Cox regression was significantly reduced compared with that of controls (for *bIrs2*$^{+/-}$, a 14-fold reduction, $P < 10^{-11}$; for *bIrs2*$^{-/-}$, a sixfold reduction, $P < 10^{-5}$) (Fig. 3A and table S3). With parametric regression, we found that the median life spans for *bIrs2*$^{+/-}$ and *bIrs2*$^{-/-}$ mice were 18% and 14% longer, respectively, than life spans for controls (for *fIrs2*, median = 791 days and 95% CI 731 to 796; for *bIrs2*$^{+/-}$, median = 936 days and 95% CI 923 to 945; for *bIrs2*$^{-/-}$, median = 901 days and 95% CI 888 to 919); the maximum life spans (90th percentile) increased similarly (Fig. 3A and table S4).

To determine whether brain Irs2 affects systemic metabolism, we studied young and old mice in a comprehensive lab animal monitoring system (CLAMS). Young control (*fIrs2*) mice were more active and consumed more oxygen than did young *bIrs2*$^{+/-}$ or *bIrs2*$^{-/-}$ mice (Fig. 3, B and C). Oxygen consumption by old *fIrs2* and *bIrs2*$^{+/-}$ mice declined to the same amount, whereas the *bIrs2*$^{-/-}$ mice consumed slightly less oxygen (Fig. 3B). All the mice were less active at 22 months; however, the old *bIrs2*$^{+/-}$ and *bIrs2*$^{-/-}$ mice were about twice as active as the old controls (Fig. 3C).

Next we determined the respiratory quotient ($R_q = VCO_2/VO_2$, where V is volume) to estimate the daily transition between fat ($R_q = 0.7$) and carbohydrate ($R_q = 1$) oxidation (*19*). The R_q for

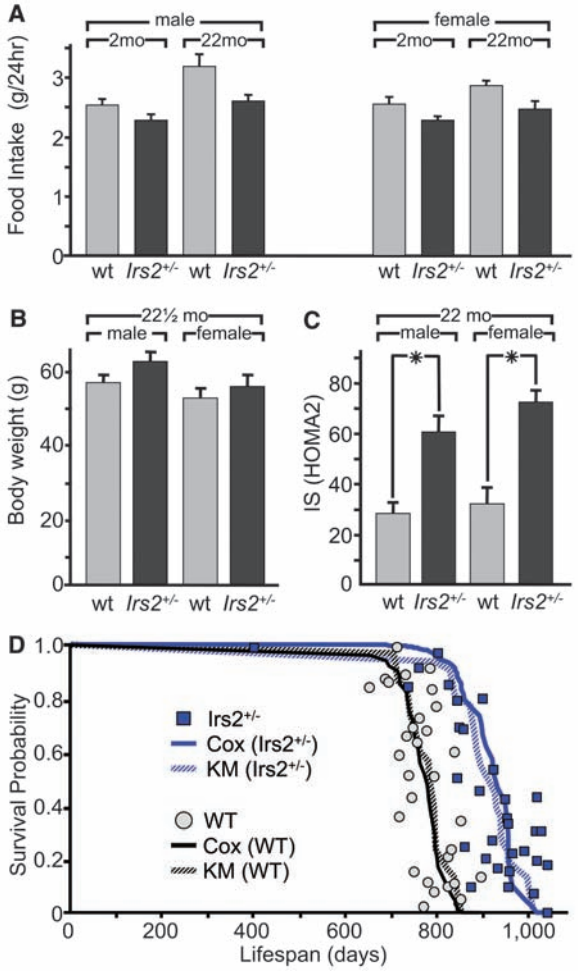

Fig. 1. Metabolism and life span of *Irs2*$^{+/-}$ mice. (**A**) Food intake [average (g/24 hour) ± SEM, n = 6 mice] in male or female mice at 2 and 22 months of age. (**B**) Body weight [average (g) ± SEM, n = 6] at 22½ months. (**C**) HOMA2 (homeostatic model assessment) of insulin sensitivity (IS) (average ± SEM, n = 8, *P < 0.05). (**D**) Survival probability was determined by Cox regression for each WT (●) and *Irs2*$^{+/-}$ (■, blue) mouse. Solid lines indicate the Cox survival probability of WT and *Irs2*$^{+/-}$ mice controlled for other covariates (see table S3 for details). Hatched lines correspond to Kaplan-Meier (KM) estimates obtained by parametric regression (see table S4 for details).

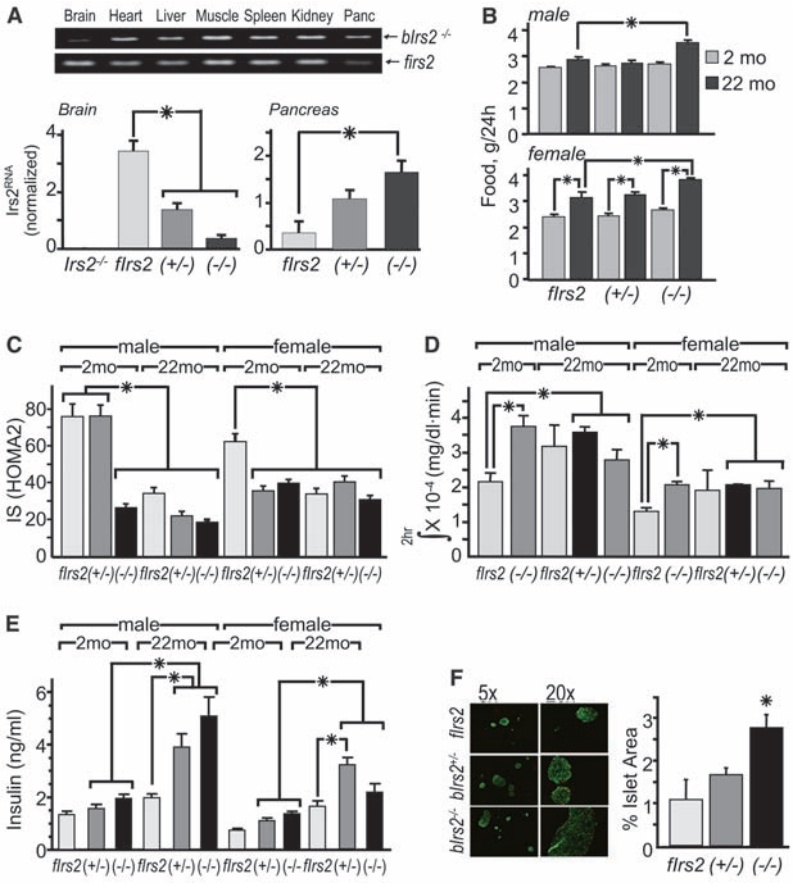

Fig. 2. Reduced neuronal Irs2 causes peripheral insulin resistance. (**A**) (Top) RT-PCR of *Irs2* RNA in mouse tissues and (bottom) quantitative RT-PCR (normalized ± SEM; $n = 5$; $^*P < 0.05$) in brain and pancreas ($Irs2^{-/-}$ indicates systemic $Irs2^{-/-}$ mice). (**B**) Food intake [average (g/24 hour) ± SEM; $n = 6$; $^*P < 0.05$] at 2 months and 22 months of age. (**C**) HOMA2 of IS (average ± SEM, $n = 8$; $^*P < 0.05$). (**D**) Average area (±SEM; $n = 6$; $^*P < 0.05$) under the blood glucose clearance curve. (**E**) Fasted insulin concentrations (±SEM, $n = 14$ to 16; $^*P < 0.05$). (**F**) (Left) Pancreas sections from 22-month-old mice were immunostained with antibody against insulin (green) or glucagon (red), and (right) the amount of islet β cell area (average ± SEM, $n = 6$ sections; $^*P < 0.05$).

all the young mice displayed the usual diurnal rhythm, which approached the maximum value during the dark cycle (Fig. 3D). By contrast, old *fIrs2* mice lost the diurnal rhythm; the R_q was indistinguishable between light and dark cycles (Fig. 3D). However, the R_q for old $bIrs2^{+/-}$ and $bIrs2^{-/-}$ mice increased significantly during the dark cycle, revealing a more youthful transition between fat and carbohydrate oxidation (Fig. 3D). Indeed, healthy long-lived humans also display a higher R_q that is closer to the value of healthy middle-aged adults (*20*).

Oxidative stress is associated with a reduced life span, and many enzymes protect cells from oxidative stress, especially superoxide dismutase (Sod) (*3*, *4*, *21*). In mice, FoxO1 promotes the expression of Sod2, so we investigated whether reduced neuronal Irs2 might help maintain brain Sod2 concentrations during feeding. Sod2 and FoxO1 protein was measured by immunoblotting hypothalamic lysates from young and old mice before and 2 hours after feeding (Fig. 4A). The Sod2 concentrations were not changed by feeding the young mice; however, Sod2 decreased at least 50% in the old fed control mice (Fig. 4, A and B). By contrast, Sod2 was not reduced by feeding old $bIrs2^{+/-}$ and $bIrs2^{-/-}$ mice (Fig. 4, A and B). A similar pattern was observed for FoxO1 levels in young and old hypothalamic tissues (Fig. 4, A and C). Thus, hypothalamic Sod2 reveals a more youthful response to feeding in mice with reduced brain Irs2.

Together, our results show that reduced Irs2 signaling in all tissues ($Irs2^{+/-}$) or just in the brain ($bIrs2^{+/-}$) increases the life spans of mice maintained on a high-energy diet about 5 months and about 4 months in $bIrs2^{-/-}$ mice (table S4). Some studies show that calorie restriction, reduced body size, and increased peripheral insulin sensitivity extend mammalian life span (*5*, *22*).

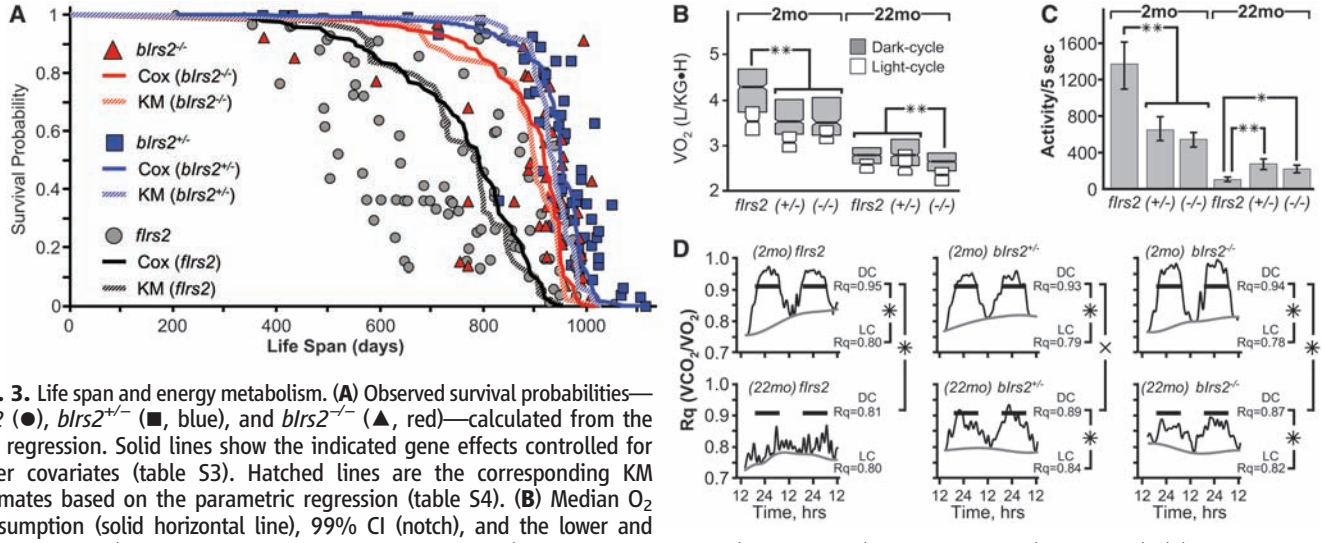

Fig. 3. Life span and energy metabolism. (**A**) Observed survival probabilities—*fIrs2* (●), $bIrs2^{+/-}$ (■, blue), and $bIrs2^{-/-}$ (▲, red)—calculated from the Cox regression. Solid lines show the indicated gene effects controlled for other covariates (table S3). Hatched lines are the corresponding KM estimates based on the parametric regression (table S4). (**B**) Median O_2 consumption (solid horizontal line), 99% CI (notch), and the lower and upper quartiles ($n = 425$ for each genotype, $^{**}P < 0.0001$) by male mice in dark (shaded boxes) and light cycles (open boxes). (**C**) Median voluntary movement (±95% CI) for male mice measured during a 5-s interval in the dark cycle ($n = 425$ for each genotype, $^*P < 0.02$, $^{**}P < 0.0001$). (**D**) Average R_q (VCO_2/VO_2) determined during 48 hours from six male mice of the indicated age and genotype. Median R_q determined in dark (DC, black bar) and light (LC) cycles (Kruskal-Wallis nonparametric test: $^*P < 0.0001$; $^{\times}P = 0.03$).

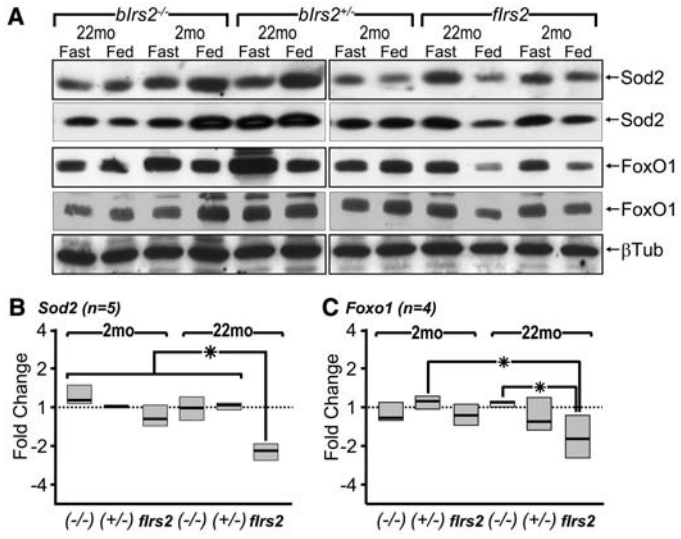

Fig. 4. Loss of brain Irs2 stabilizes Sod2 in the postprandial brain. (**A**) Hypothalamic lysates were prepared from pairs of male siblings of the indicated genotype before (Fast) or after 2-hour feeding (Fed), resolved by SDS polyacrylamide gel electrophoresis, and immunoblotted with antibodies against Sod2 or FoxO1 (two independent experiments are shown). β-tubulin (shown for one experiment) was immunoblotted for all the experiments to confirm equivalent loading. Autoradiographs were quantified, and the ratio of intensities (Fed/Fast) for (**B**) Sod2 ($n = 5$) or (**C**) FoxO1 ($n = 4$) was calculated. Boxes show the median ratio (solid horizontal line) and the lower and upper quartiles; the Kruskal-Wallis nonparametric test was used to compare the groups across all genotypes (*$P < 0.05$).

However, our long-lived mice are slightly larger and consume about the same or slightly more food than the short-lived controls. Indeed, long-lived systemic $Irs2^{+/-}$ mice are more insulin sensitive and glucose tolerant than WT mice; however, long-lived brain-specific $bIrs2^{+/-}$ and $bIrs2^{-/-}$ mice are insulin resistant, hyperinsulinemic, and glucose intolerant. The mechanism responsible for this disparity is unknown. Regardless, our results point to the brain as the site where reduced insulin-like signaling can have a consistent effect to extend mammalian life span—as it does in *C. elegans* and *D. melanogaster* (*1*, *3*).

As mammals age, compensatory hyperinsulinemia usually develops to maintain glucose homeostasis and prevent the progression toward life-threatening type 2 diabetes (*6*); however, increased circulating insulin might have negative effects on the brain that can reduce life span (*4*, *21*, *23*). By directly attenuating brain Irs2 signaling, an aging brain can be shielded from the negative effects of hyperinsulinemia that ordinarily develop with overweight and advancing age. Consistent with this hypothesis, moderate daily exercise, calorie restriction, and weight loss—which reduce circulating insulin—might increase life span by attenuating Irs2 signaling in the brain. Other strategies that improve peripheral insulin sensitivity, such as reduced growth hormone signaling, could have the same effect (*5*). Indeed, human centenarians display increased peripheral insulin sensitivity and reduced circulating insulin concentrations (*23*). Hence, we suggest that the Irs2 signaling cascade in the brain integrates the effects of peripheral nutrient homeostasis with life span.

References and Notes

1. K. A. Hughes, R. M. Reynolds, *Annu. Rev. Entomol.* **50**, 421 (2005).
2. R. A. Miller, *J. Am. Geriatr. Soc.* **53**, S284 (2005).
3. C. Kenyon, *Cell* **120**, 449 (2005).
4. D. A. Sinclair, L. Guarente, *Sci. Am.* **294**, 48 (2006).
5. M. S. Bonkowski, J. S. Rocha, M. M. Masternak, K. A. Al Regaiey, A. Bartke, *Proc. Natl. Acad. Sci. U.S.A.* **103**, 7901 (2006).
6. M. F. White, *Science* **302**, 1710 (2003).
7. D. J. Clancy *et al.*, *Science* **292**, 104 (2001).
8. D. S. Hwangbo, B. Gershman, M. P. Tu, M. Palmer, M. Tatar, *Nature* **429**, 562 (2004).
9. D. J. Withers *et al.*, *Nature* **391**, 900 (1998).
10. D. J. Withers *et al.*, *Nat. Genet.* **23**, 32 (1999).
11. D. W. Hosmer Jr., S. Lemeshow, *Applied Survival Analysis* (Wiley, New York, 1999).
12. R. W. Gelling *et al.*, *Cell Metab.* **3**, 67 (2006).
13. X. Lin *et al.*, *J. Clin. Investig.* **114**, 908 (2004).
14. T. L. Parkes *et al.*, *Nat. Genet.* **19**, 171 (1998).
15. C. A. Wolkow, K. D. Kimura, M.-S. Lee, G. Ruvkum, *Science* **290**, 147 (2000).
16. D. J. Burks *et al.*, *Nature* **407**, 377 (2000).
17. A. I. Choudhury *et al.*, *J. Clin. Investig.* **115**, 940 (2005).
18. M. Schubert *et al.*, *J. Neurosci.* **23**, 7084 (2003).
19. Y. Wang *et al.*, *Physiol. Genomics* **27**, 131 (2006).
20. M. R. Rizzo *et al.*, *J. Clin. Endocrinol. Metab.* **90**, 409 (2005).
21. H. Kabil, L. Partridge, L. G. Harshman, *Biogerontology* **8**, 201 (2007).
22. R. A. Miller, J. M. Harper, A. Galecki, D. T. Burke, *Aging Cell* **1**, 22 (2002).
23. M. Barbieri *et al.*, *Exp. Gerontol.* **38**, 137 (2003).

24. We thank R. Leshan, K. Martin, C. Aubin, N. Fujii, and V. Petkovana for technical assistance and C. Lee, J. Elmquist, M. Anderson, and H. Feldman for helpful advice. This work was supported by NIH (grants DK55326 and DK38712 to M.F.W.), the Japan Society for the Promotion of Science (A.T.), and the Yamada Science Foundation (A.T.). M.F.W. is an investigator at the Howard Hughes Medical Institute.

Supporting Online Material

www.sciencemag.org/cgi/content/full/317/5836/369/DC1
Materials and Methods
Figs. S1 to S3
Tables S1 to S4
References

6 March 2007; accepted 13 June 2007
10.1126/science.1142179

Patched1 Regulates Hedgehog Signaling at the Primary Cilium

Rajat Rohatgi,[1,2]* Ljiljana Milenkovic,[1]* Matthew P. Scott[1]†

Primary cilia are essential for transduction of the Hedgehog (Hh) signal in mammals. We investigated the role of primary cilia in regulation of Patched1 (Ptc1), the receptor for Sonic Hedgehog (Shh). Ptc1 localized to cilia and inhibited Smoothened (Smo) by preventing its accumulation within cilia. When Shh bound to Ptc1, Ptc1 left the cilia, leading to accumulation of Smo and activation of signaling. Thus, primary cilia sense Shh and transduce signals that play critical roles in development, carcinogenesis, and stem cell function.

The Hedgehog (Hh) signaling pathway plays an important role both in embryonic development and in adult stem cell function (*1*, *2*). Dysregulation of the pathway causes birth defects and human cancer (*2*). Despite the importance of Hh signaling in mammals, there are gaps in our understanding of early events in this pathway. In the absence of signal, the transmembrane protein Patched1 (Ptc1) keeps the pathway turned off by inhibiting the function of a second transmembrane protein, Smoothened (Smo). The secreted protein Sonic Hedgehog (Shh) binds and inactivates Ptc1, allowing activation of Smo. Smo then triggers target gene transcription through the Gli family of transcription factors. The mechanism by which Shh inhibits Ptc1 and Ptc1 inhibits Smo is not understood in mammals.

In *Drosophila*, Ptc inhibits the movement of Smo to the plasma membrane. Binding of Hh causes the internalization of Ptc from the plasma

[1]Departments of Developmental Biology, Genetics, and Bioengineering and Howard Hughes Medical Institute, Stanford University School of Medicine, Stanford, CA 94305, USA. [2]Department of Oncology, Stanford University School of Medicine, Stanford, CA 94305, USA.

*These authors contributed equally to this work.
†To whom correspondence should be addressed. E-mail: mscott@stanford.edu